



Electrical and Optical Properties of Well-Aligned Ho³⁺-Doped ZnO Nanorods as an Alternative Transparent Conducting Oxide

HAKAN ÇOLAK ^{1,3} and ERCAN KARAKÖSE²

1.—Faculty of Science, Department of Chemistry, Çankırı Karatekin University, 18100 Çankırı, Turkey. 2.—Vocational College, Kayseri University, 38039 Kayseri, Turkey. 3.—e-mail: hakancolak@karatekin.edu.tr

In this study, the impacts of doping concentration on the crystal structure, morphology, electrical, and optical properties of Ho³⁺-doped zinc oxide (ZnO) nanorod (NR) arrays were studied. Structural and morphological characterizations showed that the Ho³⁺-doped ZnO NRs were crystallized in the (002) direction, and that they had a homogeneous distribution on the substrate. The crystallite sizes of the samples were between 50 nm and 65 nm. SEM analysis showed that every sample was hexagonal in shape. For the 1 and 5 mol.% Ho³⁺-doped ZnO NRs, the values for electrical conductivity were found to be 1.41×10^{-7} and 8.29×10^{-6} ($\Omega \text{ cm}$)⁻¹ at 25°C and 1.70×10^{-5} and 1.24×10^{-3} ($\Omega \text{ cm}$)⁻¹ at 300°C, respectively. The optical transmittances were between 80 and 93% for all the samples in the region from 400 to 1000 nm. The optical band gap values were determined to be between 3.180 and 3.195 eV.

INTRODUCTION

Transparent conducting oxides (TCOs) are important factors in many modern devices, such as solar cells, optics, sensors, and touch screens.¹ In the modern world, the necessity for all technologies has been increasing from day to day. The intensive usability of TCOs in modern instruments, the high cost of available TCO materials, and the potential prospects for future practices has focused researchers' interests on different TCO materials.² Metal oxides with high electrical conductivity and optical transmittance can be considered to be TCO materials. The metal oxides are also described as oxide semiconductors with high band gap energy. The optical and electrical aspects of the materials can be tailored by doping with other elements. To be accepted as a TCO, the material needs to have high electrical conductivity and optical transparency in the visible range (higher than 80%).³

Fluorine-doped SnO₂ (FTO) and tin-doped In₂O₃ (ITO), which have excellent electrical and optical properties, are the most widely preferred TCO materials in current technologies. ZnO is an alternative TCO material with low cost, high durability,

non-toxicity, and abundance in nature.⁴ ZnO has a direct and wide band gap energy in the ultra violet region.⁵ To achieve the highest electrical conductivity, investigating suitable doping elements and optimal doping concentrations are important processes in improving ZnO based TCOs.¹ The performance of the dopant element depends on its ionic radius and electronegativity. Regarding ZnO materials, it is thought that doping is effective when Zn²⁺ ions are replaced by metal ions with higher valence.⁶ To improve the ZnO's electrical and optical properties, trivalent metal ions have been usually preferred as the most suitable doping elements.⁷

Nowadays, rare earth (RE) metal ions (trivalent) are often preferred as dopants for many practices due to their high electrical conductivity and optical transmittance features based on the electronic transitions occurring within the 4f energy shells.⁸ He et al.⁹ produced Sm doped ZnO thin films via chemical solution deposition. They observed that the electrical conductivity and optical transmittance firstly increased and then decreased with an increasing doping amount. The conductivity of the samples firstly increased from ~ 17.83 to ~ 357.14 ($\Omega \text{ cm}$)⁻¹ and then decreased to ~ 113.64 ($\Omega \text{ cm}$)⁻¹ with increasing doping concentration. The electrical conductivity increased due to the increasing large

carrier concentration introduced by the trivalent Sm^{3+} ion. Pandey et al.¹⁰ synthesized undoped and Eu, La, and Ce-doped ZnO nanoparticles by the sol-gel method. They observed among the three RE ions that the ZnO sample with 1 mol.% Eu had a higher electrical conductivity. Albert Manoharan et al.¹¹ synthesized undoped as well as Mn and Nd co-doped ZnO via the sol-gel method. They calculated the optical band gap values for the undoped and Mn and Nd co-doped samples as ~ 3.27 and 3.20 eV, respectively. In addition, for the samples, the electrical conductivity value was measured through the Hall effect systems, and determined that the intrinsic donor content in the sample was decreased with increasing Nd co-doping amount, which cause a further decrease in the electrical conductivity of the produced sample.¹¹ Zafar et al.¹² produced La-doped ZnO (at concentrations of 0, 2, 5, and 10 mol.%) thin films on an FTO glass substrate via the sol-gel method. The samples' electrical properties were determined by Hall measurement. They found that the conductivity increased for 2 and 5 mol.% La, and decreased for 10 mol.% La doping content. The electrical conductivity increased due to the increase in the large carrier content introduced by the La^{3+} ions. The excessive impact of charged ions in the ZnO lattice can influence the electron drift speed, low-field mobility, and diffusion parameter, which together reduce the conductivity.

Previously, we synthesized Tm_2O_3 -doped ZnO and determined that the limit of the solubility of Tm_2O_3 in the ZnO was 4 mol.%. We determined that the samples' electrical conductivity values increased with an increase in the temperature and Tm_2O_3 doping amount. The electrical conductivity values of the 4 mol.% Tm_2O_3 -doped ZnO samples at 100 and 1000°C were found to be 3.1×10^{-6} and 3.39 ($\Omega \text{ cm}$)⁻¹, respectively.¹³ In another study, sol-gel and hydrothermal methods were used to synthesize Tm^{3+} ion-doped ZnO NR thin films. The electrical conductivity values were found to be 9.74×10^{-7} and 9.71×10^{-5} ($\Omega \text{ cm}$)⁻¹ for 5 mol.% Tm^{3+} content at 25 and 300°C , respectively.¹⁴ In another work, Lu^{3+} -doped ZnO NR thin films were fabricated. The electrical conductivity values for the 5 mol.% Lu^{3+} sample were calculated to be 1.03×10^{-7} and 9.66×10^{-7} ($\Omega \text{ cm}$)⁻¹ under an air atmosphere at 25 and 300°C , respectively.¹⁵ Electrical measurements of Ho and Y-doped ZnO samples demonstrated that the resistivity values were $\sim 10^5$ and 10^4 ($\Omega \text{ cm}$), respectively.¹⁶

In the literature, there are a few studies about holmium-doped ZnO,^{17–20} but there is no study about the electrical conductivity properties of the Ho-ZnO system. With the motivation that optical transmittance and high electrical conductivity are important for TCO materials, holmium (III)-doped ZnO NRs were produced via a combination of the sol-gel spin coating and hydrothermal methods. The samples were identified by XRD (X-ray diffraction), FE-SEM (field emission-scanning electron

microscopy), 4 PPS (four point probe system) and UV-Vis (ultraviolet-visible) spectrophotometry regarding their structure, morphology, electrical conductivity, and optical transmittance, respectively.

EXPERIMENTAL

Synthesis of the Samples

The undoped and Ho^{3+} ion-doped ZnO NRs were synthesized in two steps via the methods of sol-gel spin coating and hydrothermal. Firstly, the pre-cleaned glass substrate was coated with a ZnO seed layer. To prepare the coating solution, zinc acetate dihydrate [$\text{Zn}_2\text{CH}_3(\text{COO})\cdot 2\text{H}_2\text{O}$], monoethanolamine [MEA, $\text{NH}_2\text{CH}_2\text{CH}_2\text{OH}$], and 2-methoxyethanol [$\text{CH}_3\text{OCH}_2\text{CH}_2\text{OH}$] were the sources, respectively, for the Zn^{2+} ions, stabilizer, and solvent. For the coating solution, the concentration of Zn^{2+} was 0.5 M (molar, mol/liter) and the Zn^{2+} /MEA molar ratio was adjusted to 1:1. In the spin coating process, 1 ml of the solution was dropped on the substrate and rotated at 3000 rpm for 30 s. For 15 min, the obtained films were pre-heated to 250°C to remove the solvent. The procedure for the pre-heating and coating was repeated 5 times. At the end of this step, the seed substrate was then annealed at 450°C for 12 h, for complete crystallization.

In the second step, the undoped and Ho^{3+} ion-doped ZnO NRs were grown via the hydrothermal method on the substrates that had been seeded. Hydrothermal reactions were performed in a Teflon-coated autoclave made of stainless steel. As starting materials, zinc nitrate hexahydrate [$\text{Zn}(\text{NO}_3)_2\cdot 6\text{H}_2\text{O}$], hexamethylenetetramine [HMT, $\text{C}_6\text{H}_{12}\text{N}_4$] and holmium chloride hexahydrate [$\text{HoCl}_3\cdot 6\text{H}_2\text{O}$] were used as the source of the Zn^{2+} ions, solvent, and holmium ions, respectively. The zinc nitrate was dissolved in deionized water. The concentration of the solution was 0.075 M. Then there was the addition of HMT into the solution (molar ratio with Zn^{2+} was 1:1). Lastly, holmium chloride was added into the solution, so the $[\text{Ho}^{3+}]/[\text{Zn}^{2+} + \text{Ho}^{3+}]$ ratios were in the range of 0–5 mol.%. The seeded substrate was placed in the final solution with the seeded surface downward at an angle of 45° in an autoclave. The hydrothermal processes were undertaken at 95°C for 4 h.

Characterizations

The samples were characterized by XRD, FE-SEM, UV spectrophotometry and 4 PPS. The measurements for the electrical conductivity were made at between 25 and 300°C in a sealed test chamber filled with an air atmosphere. The coated substrates were centered in the chamber for the electrical conductivity measurements. So that the contact resistance could be reduced, the surface had fine platinum wires attached directly. The wires had 0.2-

cm contact separations and were located symmetrically with relation to the substrate's center. Keithley 2400 and 2700 devices were used to obtain the measurements. UV-Vis measurements of the samples were made using a spectrophotometer at room temperature in the 300- to 1000-nm wavelength range.

RESULTS AND DISCUSSION

Structural and Morphological Analysis

The crystal structure of the samples was examined by an XRD operating in Bragg-Brentano geometry over a $10^\circ \leq 2\theta \leq 90^\circ$ angular range. Figure 1a gives the XRD patterns of all the samples. All the patterns, except for the patterns of the 3 and 4 mol.% doped, have two peaks that correspond to the planes (002) and (004). The samples with 3 and 4 mol.% doped only have the (002) peak. In all the cases, all observed peaks were indexed as wurtzite (hexagonal) structures (PDF Card No: 36-1451). The (002) peaks, which were very strong, indicated that the direction of the growth was *c*-axis for the nanorod films, confirming a highly textured deposit and one dimensional (1D) structure. The orientation along the (002) direction of ZnO is preferential and suitable in terms of the thermodynamic features, as growth in the (002) direction procures the lowest energy configuration.²¹ The XRD patterns demonstrate that the Ho³⁺ doped samples do not have any secondary phases, changes in the crystal structure, or impurity peaks, which show that the dopant is well integrated into the ZnO lattice. The high-intensity peaks indicated that the crystals were of high quality.

Crystal deformity due to native point defects, such as interstitial atoms and vacancies, may lead to the XRD peak shifting towards higher or lower 2θ angles. The magnified view of the patterns of the (002) peaks is shown in Fig. 1b; the position and intensity of the (002) peak gradually shifted toward the lower 2θ angles and slightly increased with higher doping concentration, respectively. This demonstrates that the Ho³⁺ ions have been successfully joined into the ZnO lattice. A similar trend has been reported by other studies.^{20,22,23}

In addition, the unit cell constant of *c* can be calculated using the following formula from the (002) diffraction peaks:²⁴

$$\frac{1}{d^2} = \frac{4}{3} \left(\frac{h^2 + hk + k^2}{a^2} \right) + \frac{l^2}{c^2} \quad (1)$$

where *d* is the lattice spacing. The *c* values of the Ho³⁺ ion-doped ZnO NRs are shown in Table I; it can be seen that the *c* constant became greater with increasing doping concentration. The ionic radii (six-coordinate) of the Zn²⁺ and Ho³⁺ ions were 0.74 and 1.041 Å, respectively.²⁵ The increase in the *c* parameter of the lattice is an indication of the substitution of the Zn²⁺ cations (which have smaller

radius) with Ho³⁺ ions (which have larger radius) in the ZnO crystal lattice. This meant that there was an increase in the parameters of the lattice as there was the substitution of the larger radius ion with the smaller one. In our previous reports, we synthesized Tm³⁺ and Lu³⁺ ion-doped ZnO NRs, and the parameters increased with the doping concentration.^{14,15} The result is in good agreement with Singh et al.¹⁶ When the ionic radius of the doping ion increases, the lattice constants increase and the XRD peaks shift towards lower angles. We meant that in the range of 0 and 5 mol.% doping concentration, all the results such as having no any secondary phases, no changes in the crystal structure, no impurity phases, shifting of the (002) peak toward a lower angle and increase in the unit cell parameter confirm that the Ho³⁺ ions have been successfully incorporated into the ZnO crystal lattice.

For the ZnO samples, the average crystallite sizes (*D*), were estimated using the Scherrer relationship from the (002) peak²⁶:

$$D = \frac{0.9\lambda}{\beta \cos\theta} \quad (2)$$

where λ is the wavelength of the X-rays (CuK α = 1.542 Å), β is the full width at half-maximum (FWHM) and θ is the diffraction angle. It was found that the crystallite size increased with the addition of Ho³⁺ doping owing to the decrease in the FWHM, according to the Ho³⁺ doping concentration (Table I).

The texture coefficient (TC) has important details related to the deposition of the thin film and its preferred orientation. TC_(hkl) can be calculated from the XRD patterns using the following relationship:

$$TC_{(hkl)} = \frac{I_{(hkl)}/I_{0(hkl)}}{1/n \left[\sum_n I_{(hkl)}/I_{0(hkl)} \right]} \quad (3)$$

where *n* is the number of diffraction peaks with respect to the JCPDS reference data, *I*_(hkl) is the experimental intensity, and *I*_{0(hkl)} is the reference intensity.²⁷ The TC_(hkl) indicates the texture of a significant direction; deviation of a direction from the ideal structure exhibits the growth direction that is preferred. The TC₍₀₀₂₎ values are given in Table I. It can be said that the Ho³⁺-doped ZnO NRs clearly grew along the (002) direction. The texture decreases for the 3, 4 and 5 mol.% doped samples due to the melting and decomposition/agglomeration of the rod structures with the heating treatment (see the SEM section). With respect to the different JCPDS card numbers about ZnO samples (36-1451; 65-3411; 01-070-8070) *n* should be 13. If the value of the TC_(hkl) is equal to *n*, then the sample is excellently oriented in the (002) direction (single crystal behavior). Therefore, it can be said that the Ho³⁺ ion-doped ZnO NR samples have a single crystal behavior.

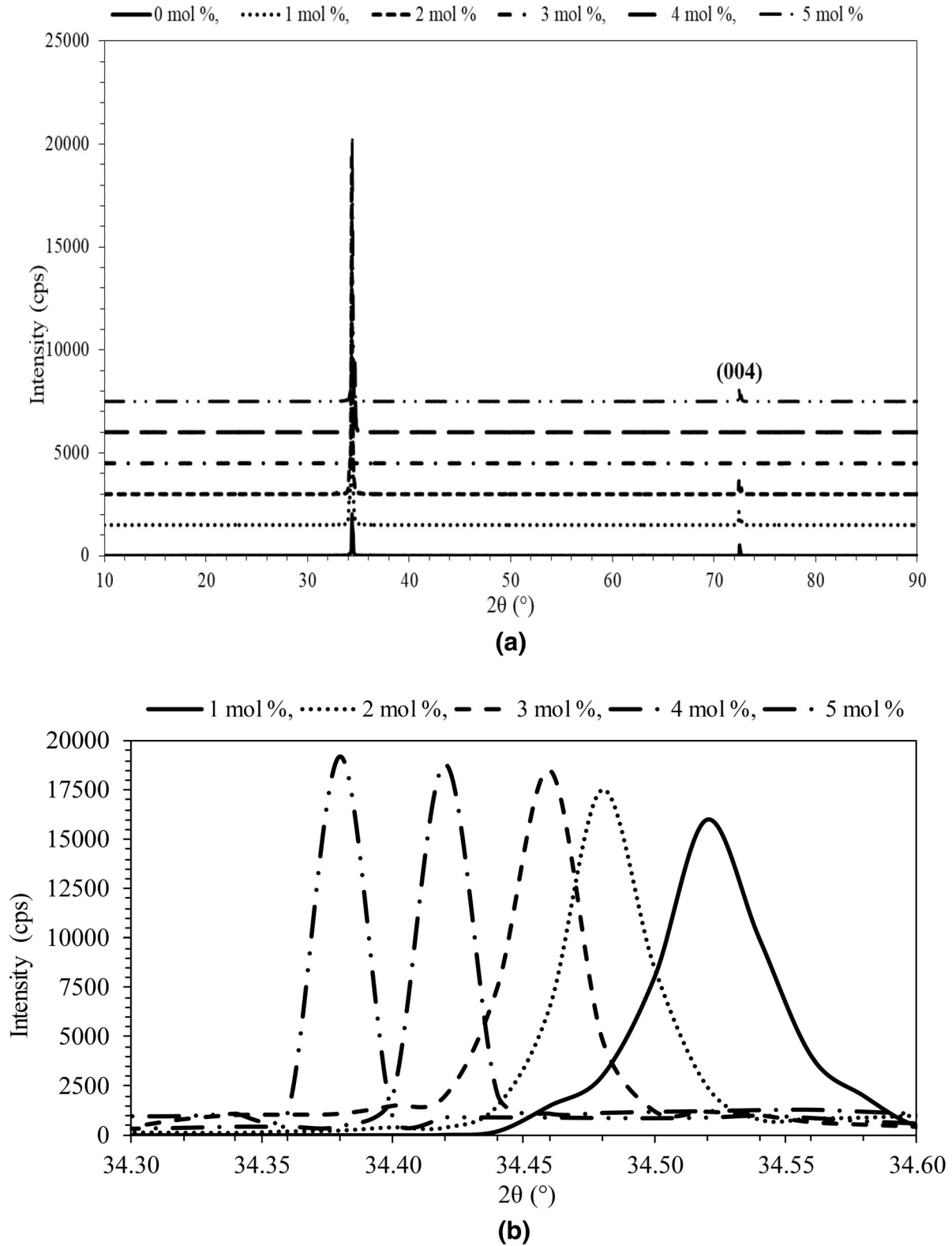


Fig. 1. (a) XRD patterns of ZnO nanorod samples. (b) Shifts in (002) peak position of ZnO nanorod samples.

Table I. Unit cell parameters, crystallite size, texture coefficient, activation energy, and band gap energy values of ZnO samples

Sample name	Unit cell parameters (Å)		Crystallite size [D (nm)]	Texture coefficient (TC ₍₀₀₂₎)	Activation energy (E _a , eV)	Band gap energy (E _g , eV)
	a	c				
Undoped ZnO	–	5.150	65	9.450	0.140	3.195
1 mol.% Ho ³⁺ -ZnO	–	5.153	62	10.605	0.220	3.190
2 mol.% Ho ³⁺ -ZnO	–	5.172	57	10.700	0.221	3.187
3 mol.% Ho ³⁺ -ZnO	–	5.185	55	9.730	0.235	3.183
4 mol.% Ho ³⁺ -ZnO	–	5.199	51	9.160	0.232	3.182
5 mol.% Ho ³⁺ -ZnO	–	5.223	50	8.300	0.236	3.180

Figure 2 shows the SEM images of the ZnO samples. Hexagonal shapes were observed for every sample. All the images show that on the substrate, Ho³⁺ ion-doped ZnO NRs had distributions that were homogeneous. From the micrographs for 3, 4 and 5 mol.% doped samples, it can be understood that melting was started with the effect of the heating treatment, and then the decomposition and/or agglomeration of the rod structures started. The diameter and density of the nanorods were affected by the nucleation sites. Increasing the impurity doping concentration improved the density of the nucleation. As a result, the growth rate was induced by the Ho³⁺ ion doping concentration which, in turn, results in a coarsening and lateral aggregation of the nanorods.²⁸

Electrical Conductivity Measurements

The ZnO NRs' electrical conductivity can be calculated using Eq. 4:

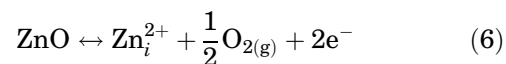
$$\sigma = \frac{I}{V} G^{-1} \quad (4)$$

where σ is the total conductivity, I is the direct current, V is the voltage and G is the geometric correction factor.²⁹ Generally, the conductivity of the semiconductor materials can be increased with temperature. This is a result of the thermally activated process. The electrical conductivity can be found using Eq. (5):

$$\sigma = \sigma_0 \exp(-E_a/kT) \quad (5)$$

where E_a , k and σ_0 are the activation energy, Boltzmann constant, and the electrical conductivity at absolute temperature (T), respectively.^{30,31} The heating treatment process can effect the ZnO NR samples' electrical properties. Thus, useful data about the possible structure and its variations of the ZnO NRs can be obtained from the electrical conductivity variation against temperature.³² With this aim, $\log \sigma$ versus $10^3/T$ plots of the ZnO NRs are shown in Fig. 3. As seen, the electrical conductivity

of the ZnO samples increased with increasing temperature. This behavior can be explained by the following mechanism:



where, Zn_i^{2+} is the interstitial Zn^{2+} ion. The two electrons released into the crystal lattice after ionization increase the concentration of the carrier. The electrical conduction in the ZnO crystal is owing to the free electrons or holes moving from one site to the next. In addition, oxygen that is adsorbed on the ZnO surface is released to the atmosphere by the heating process. ZnO is a non-stoichiometric material owing to the interstitial Zn atoms (Zn_i), and native defects formed at high temperatures.^{5,33} From the same figure, it can be seen that there is an increase in the electrical conductivity with an increase in the doping amount. The electrical conductivity values of the 0, 1 and 5 mol.% Ho³⁺ ion-doped ZnO NRs were measured as 1.94×10^{-8} , 1.41×10^{-7} , and $8.29 \times 10^{-6} (\Omega \text{ cm})^{-1}$ at 25°C and 3.58×10^{-7} , 1.70×10^{-5} , and $1.24 \times 10^{-3} (\Omega \text{ cm})^{-1}$ at 300°C, respectively. But our conductivity levels are not as high as others have found.^{9,16} Sing et al.¹⁶ observed a conductivity value of $1 \times 10^{-5} (\Omega \text{ cm})^{-1}$ for a 1 mol.% Ho-doped sample. In addition, the electrical conductivity values obtained at different measurement temperatures are shown in Table II. The increase is derived from the increase in the large carrier amount introduced by the trivalent Ho³⁺ ions.⁹ The increase can be explained as follows: Ho³⁺ ions in the ZnO crystal lattice are acting as a donor. The number of free electrons in the ZnO NRs increases with an increase in the Ho³⁺ doping amounts, because a Ho³⁺ ion has one valence electron more than Zn²⁺. It may be considered that the Ho³⁺ ion replaces the Zn²⁺ ion, or it occupies the interstitial sites. In both cases, the Ho³⁺ ion acts as a donor.

In our previous study we observed that the electrical conductivity values of the 1 and 5 mol.% Tm³⁺-doped ZnO NRs samples were 1.17×10^{-7}

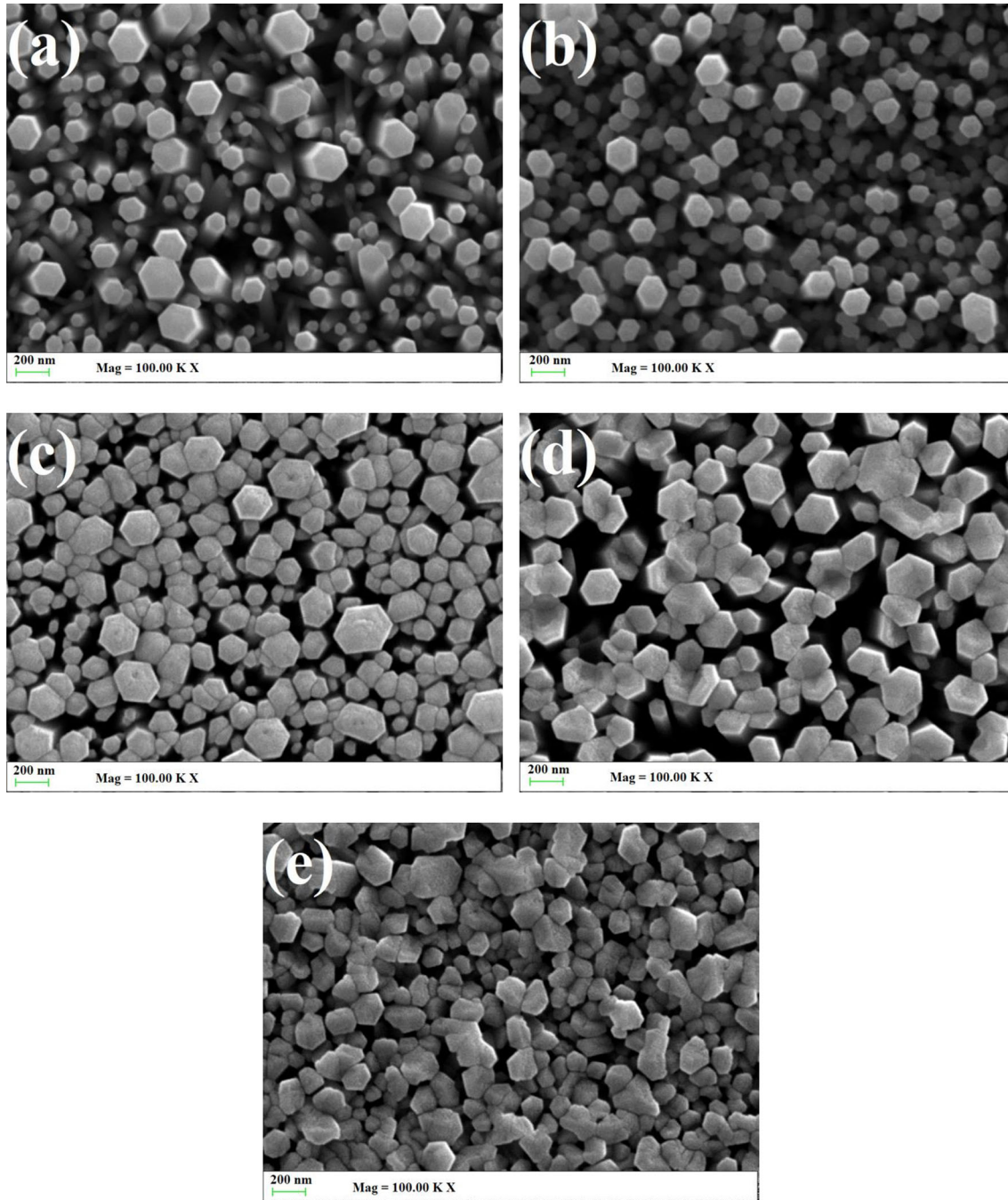


Fig. 2. Top view SEM images of ZnO nanorod samples: (a) 1, (b) 2, (c) 3, (d) 4, and (e) 5 mol.% Ho³⁺-doped.

and 9.74×10^{-7} at 25°C and 4.07×10^{-6} and 9.71×10^{-5} ($\Omega \text{ cm}$)⁻¹ at 300°C, respectively.¹⁴ In another study we found that the electrical conductivity values of the 1 and 5 mol.% Lu³⁺-doped ZnO NRs samples were 3.19×10^{-8} , 1.10×10^{-6} ($\Omega \text{ cm}$)⁻¹ at 25°C and 1.03×10^{-7} and 9.66×10^{-7} ($\Omega \text{ cm}$)⁻¹ at 300°C, respectively.¹⁵ From all the given values, it can be understood that the electrical conductivity of the Ho³⁺-doped ZnO samples are highest. The ionic radii (six-coordinate) of the Ho³⁺, Tm³⁺, and Lu³⁺ ions are 1.041, 0.870, and 0.861 Å, respectively. As the ionic radius of the Ho³⁺ is the

biggest, the attraction of the valance electrons of the Ho³⁺ ion is the weakest. Therefore, its valance electrons can be easily released in the ZnO crystal lattice.

The found *E_a* values for the undoped and Ho³⁺ ion-doped ZnO NRs are given in Table I. The activation energy values generally increase with increasing doping concentration. The sheet resistance values (Table I) of the 5 mol.% Ho³⁺ ion-doped ZnO NRs film on the glass substrate were 8.23 and 0.05 O/sq. at 25°C and 300°C, respectively. Therefore, the studied ZnO NRs thin film samples are

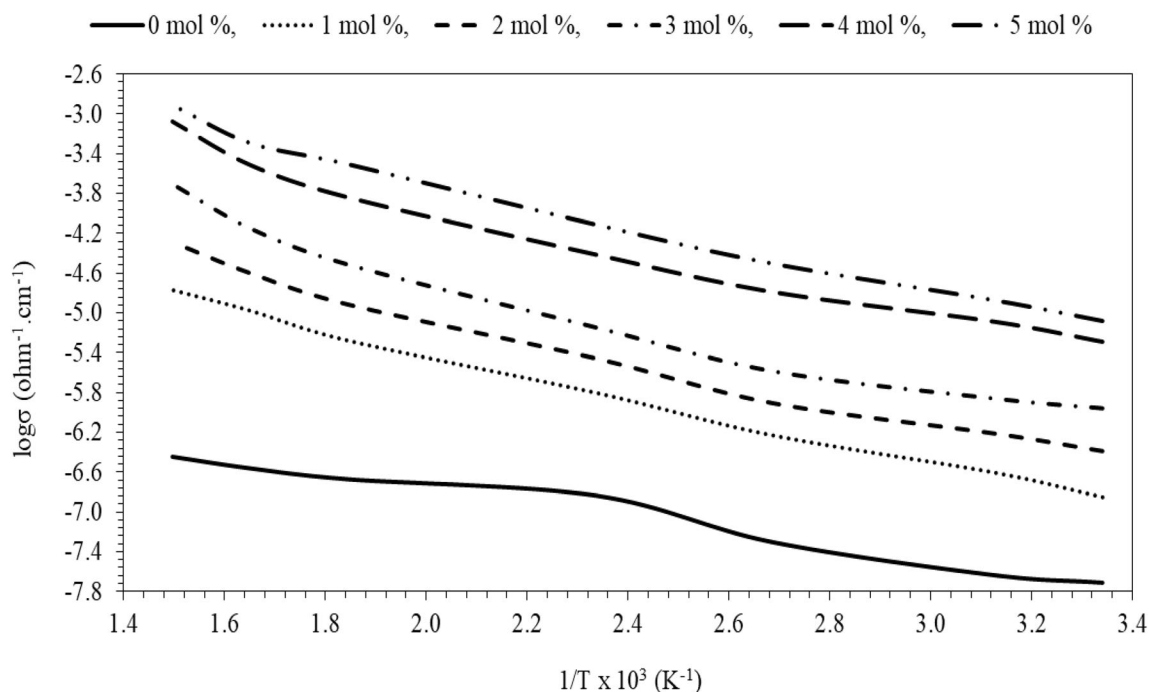


Fig. 3. Electrical conductivity graphs of ZnO nanorod samples.

Table II. Electrical conductivity, resistivity and sheet resistance values versus temperature of ZnO samples

	Temperature (°C)				Sample name
	25	100	200	300	
Conductivity ($\Omega \text{ cm}^{-1}$) ⁻¹	1.94E - 08	4.98E - 08	2.12E - 07	3.58E - 07	Undoped ZnO
	1.41E - 07	5.89E - 07	5.24E - 06	1.70E - 05	1 mol.% Ho ³⁺ -ZnO
	4.08E - 07	1.25E - 06	1.21E - 05	5.17E - 05	2 mol.% Ho ³⁺ -ZnO
	1.10E - 06	2.61E - 06	3.05E - 05	1.97E - 04	3 mol.% Ho ³⁺ -ZnO
	5.13E - 06	1.63E - 05	1.44E - 04	8.43E - 04	4 mol.% Ho ³⁺ -ZnO
	8.29E - 06	3.15E - 05	3.11E - 04	1.24E - 03	5 mol.% Ho ³⁺ -ZnO
Resistivity ($\Omega \text{ cm}$)	5.15E + 07	2.01E + 07	4.72E + 06	2.79E + 06	Undoped ZnO
	7.09E + 06	1.70E + 06	1.91E + 05	5.88E + 04	1 mol.% Ho ³⁺ -ZnO
	2.45E + 06	8.00E + 05	8.26E + 04	1.93E + 04	2 mol.% Ho ³⁺ -ZnO
	9.09E + 05	3.83E + 05	3.28E + 04	5.08E + 03	3 mol.% Ho ³⁺ -ZnO
	1.95E + 05	6.13E + 04	6.94E + 03	1.19E + 03	4 mol.% Ho ³⁺ -ZnO
	1.21E + 05	3.17E + 04	3.22E + 03	8.06E + 02	5 mol.% Ho ³⁺ -ZnO
Sheet resistance (Ω^2)	3.50E + 03	1.37E + 03	3.21E + 02	1.90E + 02	Undoped ZnO
	4.82E + 02	1.16E + 02	1.30E + 01	3.40E + 00	1 mol.% Ho ³⁺ -ZnO
	1.67E + 02	5.44E + 01	5.62E + 00	1.31E + 00	2 mol.% Ho ³⁺ -ZnO
	6.18E + 01	2.60E + 01	2.23E + 00	0.35E + 00	3 mol.% Ho ³⁺ -ZnO
	1.33E + 01	4.17E + 00	0.47E + 00	0.08E + 00	4 mol.% Ho ³⁺ -ZnO
	8.23E + 00	2.16E + 00	0.22E + 00	0.05E + 00	5 mol.% Ho ³⁺ -ZnO

comparable with commercial TCO films ($\sim 10 \text{ O/sq.}$) used in thin film solar cells, and can be considered to be promising TCO material.

Optical Studies

For the undoped and Ho³⁺ ion-doped ZnO NRs, the UV graphs are shown in Fig. 4. The transmittances are between 80 and 93% for all the samples

in the region from 400 to 1000 nm. This graph indicates that the optical transmittance increases up to 2 mol.%. The very good optical quality, with a very good crystallite and structural homogeneity for the ZnO NRs give rise to high transparency.³⁴ The transmittance slowly decreases for the 3, 4 and 5 mol.% doped samples as the melting and decomposition/agglomeration of the rod structures occurs with heating treatment (see the SEM section). In

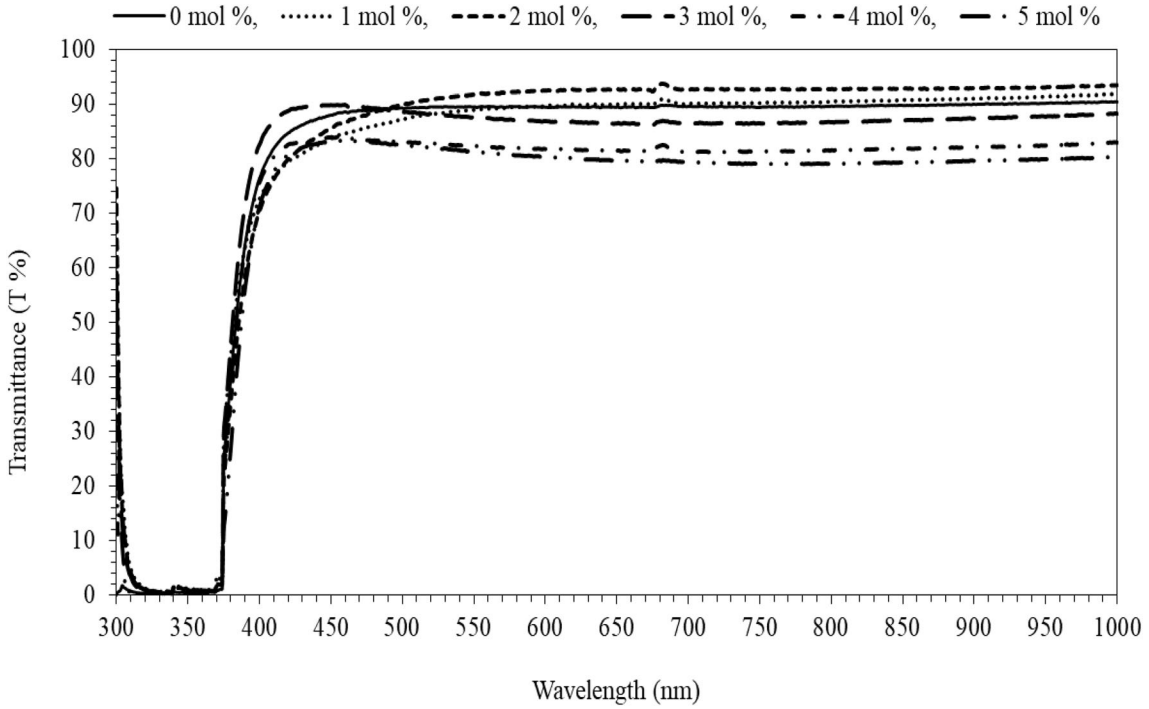


Fig. 4. UV/VIS graphs of ZnO nanorod samples.

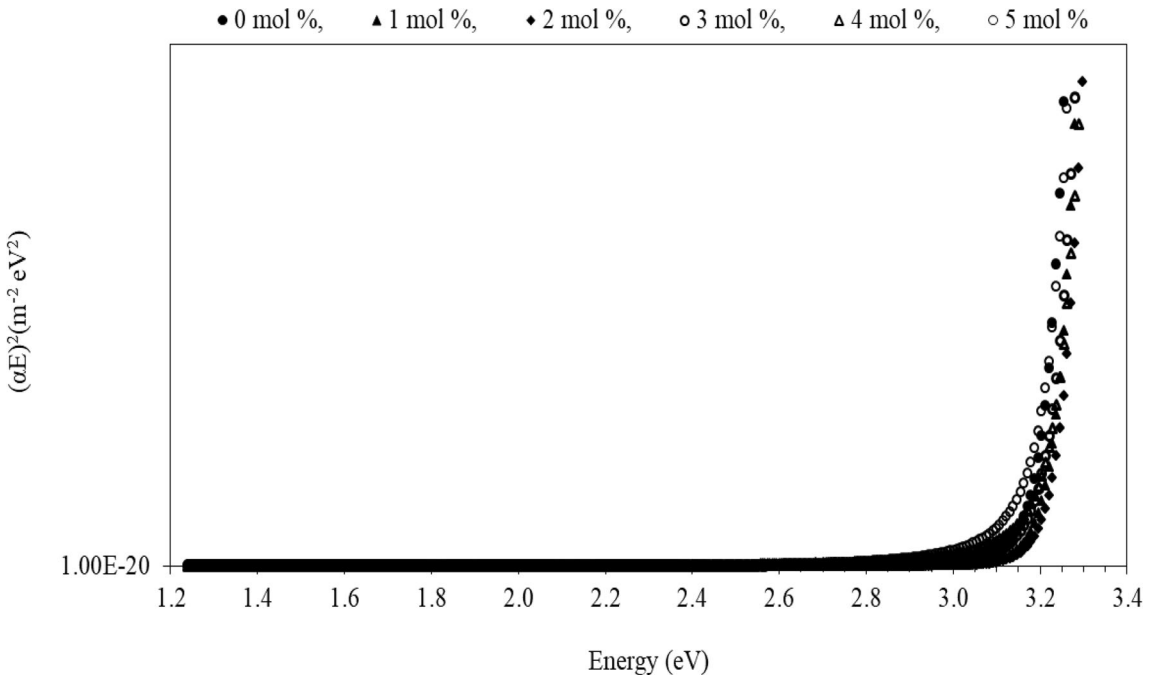


Fig. 5. Graphs of $(\alpha E)^2$ versus $(h\nu, \text{eV})$ of ZnO nanorod samples.

spite of this, all the samples have a smooth surface due to their nanorod structures. The nanorod structures allow light to pass through without scattering.

The optical band gap (E_g) was obtained from the variation in the absorption parameter (α) with

photon energy ($h\nu$). It can be calculated using the Tauc relationship, as follows:³⁵

$$\alpha(h\nu) = A(h\nu - E_g)^{1/2} \tag{7}$$

here, A is a constant. Figure 5 shows the graphs of $(\alpha E)^2$ versus photon energy ($h\nu$, eV) for all the samples. In addition, the band gap values can be seen in Table I. Doping any element in ZnO can produce distortions and results in changes in the band gap. This variation in the values originates from different parameters, such as grain size, carrier amount and positions of the dopant ions in the ZnO crystal structure.³⁶ As a native n-type oxide semiconductor, ZnO is doped by the Ho³⁺ ions, and it is anticipated that the ions behave as the donor by replacement with Zn²⁺ ions. The excess electrons ionized by the Ho³⁺ ions will fill up the conduction band minimum of the ZnO. Owing to the low density levels close to the conduction band minimum, electrons which are stimulated from the valence band by light have to occupy the higher energy state. With increasing doping concentrations, the carrier concentration increases, and the donor state corresponding to the Ho³⁺ ions in the ZnO energy band slowly enlarges and then combines with the conduction band. The joining causes a decrease in the ZnO band gap. The optical absorption edge shifts to the higher wavelength.³⁷

CONCLUSION

In this study, with an increasing Ho³⁺ ion doping concentration for the ZnO NR samples we observed a blue shift in the position of the (002) peak in the XRD pattern; an increase in the c lattice parameter; a decrease in the crystallite size from the XRD results; a melting and then decomposition/agglomeration of the rod structures with the effect of the heating treatment; an increase in the electrical conductivity and activation energy; and a decrease in the optical band gap energy. The studied ZnO NR thin film samples are comparable with commercial TCO films and can be considered as promising TCO material.

ACKNOWLEDGEMENTS

This research was financially supported by TUBITAK (The Scientific and Technological Research Council of Turkey) (Project No. 114Z572); and Çankırı Karatekin University (Project No. BAP, FF28015B12).

CONFLICT OF INTEREST

The authors whose names are listed immediately below certify that they have no affiliations with or involvement in any organization or entity with any financial interest (such as honoraria; educational grants; participation in speakers' bureaus; membership, employment, consultancies, stock ownership, or other equity interest; and expert testimony or patent-licensing arrangements), or non-financial interest (such as personal or professional relationships, affiliations, knowledge or beliefs) in the sub-

ject matter or materials discussed in this manuscript.

REFERENCES

1. B.G. Lewis and D.C. Paine, *MRS Bull.* 25, 22 (2011).
2. D.S.Y. Jayathilake and T.A. Nirmal Peiris, *SF. J. Mater. Chem. Eng.* 1, 1004 (2018).
3. C.G. Granqvist and A. Hultaker, *Thin Solid Films* 411, 1 (2002).
4. T. Minami, *Thin Solid Films* 516, 1314 (2008).
5. A.A. Janotti and C.G. Van de Walle, *Rep. Prog. Phys.* 72, 126501 (2009).
6. V. Kumari, V. Kumar, B.P. Malik, R.M. Mehra, and D. Mohan, *Opt. Commun.* 285, 2182 (2012).
7. R.A. Mereu, A. Mesaros, M. Vasilescu, M. Popa, M.S. Gabor, L. Ciontea, and T. Petrisor, *Ceram. Int.* 39, 5535 (2013).
8. A. Hastir, N. Kohli, and R.C. Singh, *J. Phys. Chem. Solid.* 105, 23 (2017).
9. H.Y. He, J. Fei, and J. Lu, *J. Nanostruct. Chem.* 5, 169 (2015).
10. P. Pandey, R. Kurchania, and F.Z. Haque, *Opt. Spectrosc.* 119, 666 (2015).
11. A. Albert Manoharan, R. Chandramohan, K. Deva Arun Kumar, S. Valanarasu, V. Ganesh, M. Shkir, H. Algarni and S. AlFaify, *J. Mater. Sci. Mater. Electron.* 29, 13077 (2018).
12. M. Zafar, B.S. Kim, and D.H. Kim, *Mater. Chem. Phys.* 240, 12207 (2020).
13. H. Çolak, *J. Mater. Sci. Mater. Electron.* 26, 784 (2015).
14. H. Çolak and E. Karaköse, *J. Rare Earth* 36, 1067 (2018).
15. H. Çolak and E. Karaköse, *Mater. Sci. Semicond. Process.* 101, 230 (2019).
16. S. Singh, J.N. Divya Deepthi, B. Ramachandran and M.S. Ramachandra Rao, *Mater. Lett.* 65, 2930 (2011).
17. M. Akyol, A. Ekicibil, and K. Kıymaç, *J. Supercond. Nov. Magn.* 26, 3257 (2013).
18. A. Ekicibil, *Solid State Sci.* 14, 1486 (2012).
19. A. Franco Jr and H.V. Pessoni, *Mater. Lett.* 180, 305 (2016).
20. A. Phuruangrat, O. Yayapao, T. Thongtem, and S. Thongtem, *Superlattices Microstruct.* 67, 118 (2014).
21. S. Yilmaz, S. Garryb, E. McGlynnb, and E. Bacaksiz, *Ceram. Int.* 40, 7753 (2014).
22. S. Aydin and G. Turgut, *Appl. Phys. A* 125, 622 (2019).
23. B. Panigrahy, M. Aslami, D.S. Misra, and D. Bahadur, *Int. J. Nanosci.* 10, 629 (2011).
24. P. Ruankham, T. Sagawa, H. Sakaguchi, and S. Yoshikawa, *J. Mater. Chem.* 21, 9710 (2011).
25. R.C. Weast, *Handbook of Chemistry and Physics*, 56th ed. (New York: CRC Press, 1975–1976), pp. 198–199.
26. A. Petterson, *Phys. Rev.* 56, 978 (1939).
27. G. Kartopu, V. Barrioz, S.J.C. Irvine, A.J. Clayton, S. Monir, and D.A. Lamb, *Thin Solid Films* 558, 374 (2014).
28. M. Babiker, D. Wang, J. Wang, Q. Li, J. Sun, Y. Yan, Q. Yu, and S. Jiao, *Nanoscale Res. Lett.* 9, 199 (2014).
29. S. Yilmaz, *J. Semicond.* 36, 082001 (2015).
30. H. Çolak, *Kovove Mater.* 54, 107 (2016).
31. A.R. West, *Solid State Chemistry and Its Applications* (New York: Wiley, 1984).
32. J.B. Lee, H.J. Le, S.H. Seo, and J.S. Park, *Thin Solid Films* 398–399, 641 (2001).
33. A. Sawalha, M. Abu-Abdeen, and A. Sedky, *Phys. B* 404, 1316 (2009).
34. A.V. Patil, C.G. Dighavkar, S.K. Sonawane, S.J. Patil, and R.Y. Borse, *Optoelectron. Adv. Mat.* 3, 879 (2009).
35. J. Tauc, *Mater. Res. Bull.* 3, 37 (1968).
36. S. Husain, L.A. Alkhtaby, E. Giorgetti, A. Zoppi, and M.M. Miranda, *J. Lumin.* 145, 132 (2014).
37. G. Tang, H. Liu and W. Zhang, *Adv. Mater. Sci. Eng.* Article ID 348601 (2013).

Publisher's Note Springer Nature remains neutral with regard to jurisdictional claims in published maps and institutional affiliations.